Cell

Parallel, Redundant Circuit Organization for Homeostatic Control of Feeding Behavior

J. Nicholas Betley,[1,2] Zhen Fang Huang Cao,[1,2] Kimberly D. Ritola,[1] and Scott M. Sternson[1,*]
[1]Janelia Farm Research Campus, HHMI, 19700 Helix Drive, Ashburn, VA 20147, USA
[2]These authors contributed equally to this work
*Correspondence: sternsons@janelia.hhmi.org
http://dx.doi.org/10.1016/j.cell.2013.11.002

SUMMARY

Neural circuits for essential natural behaviors are shaped by selective pressure to coordinate reliable execution of flexible goal-directed actions. However, the structural and functional organization of survival-oriented circuits is poorly understood due to exceptionally complex neuroanatomy. This is exemplified by AGRP neurons, which are a molecularly defined population that is sufficient to rapidly coordinate voracious food seeking and consumption behaviors. Here, we use cell-type-specific techniques for neural circuit manipulation and projection-specific anatomical analysis to examine the organization of this critical homeostatic circuit that regulates feeding. We show that AGRP neuronal circuits use a segregated, parallel, and redundant output configuration. AGRP neuron axon projections that target different brain regions originate from distinct subpopulations, several of which are sufficient to independently evoke feeding. The concerted anatomical and functional analysis of AGRP neuron projection populations reveals a constellation of core forebrain nodes, which are part of an extended circuit that mediates feeding behavior.

INTRODUCTION

Neural control of essential natural behaviors (e.g., feeding, drinking) requires coordination of flexible actions that must be robustly and reliably displayed. The relationship between circuit structure and function forms a critical framework for understanding how the brain controls natural behaviors. Because neural circuits that orchestrate survival behaviors are under strong selective pressure, they are expected to have some "hard-wired" components that can be reproducibly identified (Swanson, 2000; Tinbergen, 1989). Consequently, the prospect of uncovering dedicated neural circuits for complex, goal-directed behaviors has been a longstanding topic in genetics, neurobiology, and ethology (Hess, 1957; Stockinger et al., 2005; Tinbergen, 1989).

Consistent with the prediction of dedicated circuit components, complex survival-oriented behaviors can be evoked selectively by exogenous activation of discrete brain regions (Delgado and Anand, 1953; Hess, 1957; Kruk et al., 1983). These are some of the most dramatic behavioral responses in neuroscience, and the brain regions that can elicit distinct survival behaviors have served as entry points to elucidate the underlying neural circuits (Roeling et al., 1994; Swanson, 2000). Anatomical analysis shows that brain regions functionally associated with survival behaviors have divergent axon projections, as might be expected for coordination of complex behaviors. Yet despite widespread interconnectedness, functional dissection of the circuit pathways has been limited to simple linear relationships (Kirchgessner and Sclafani, 1988; Kow et al., 1977). The primary limitation has been that the classical tools of lesions, pharmacological injections, and electrical stimulation have been too nonspecific for comprehensive neural circuit analysis. A more complete picture would involve understanding the functional contribution of separate axon projections to the behavioral response as well as the anatomical relationship between these projection fields.

Molecularly defined neurons and their circuits offer high specificity for systematic interrogation of the relationship between circuit structure and function. We have focused on circuits involving agouti-related protein (AGRP)-expressing neurons. These are an internally oriented sensory neuron population in the hypothalamic arcuate nucleus (ARC) that reads out circulating metabolic and hormonal signals of physiological energy state (Belgardt et al., 2009). Optogenetic and chemogenetic activation of AGRP neurons is sufficient to rapidly orchestrate voracious feeding behaviors without training (Aponte et al., 2011; Krashes et al., 2011). Moreover, loss-of-function experiments led to a reduction in food consumption (Krashes et al., 2011; Luquet et al., 2005), which demonstrates that these neurons are important for natural feeding behavior. The axon projections of AGRP neurons can be selectively activated using channelrhodopsin-2 (ChR2) (Atasoy et al., 2008), and AGRP neuron projections to the paraventricular hypothalamic nucleus ($ARC^{AGRP} \rightarrow PVH$) have been shown to evoke feeding behavior (Atasoy et al., 2012). Therefore, probing the axon projections of this molecularly defined population offers an opportunity to explore the relationship between anatomical organization and functional output of a neural circuit that orchestrates a complex, natural behavior.

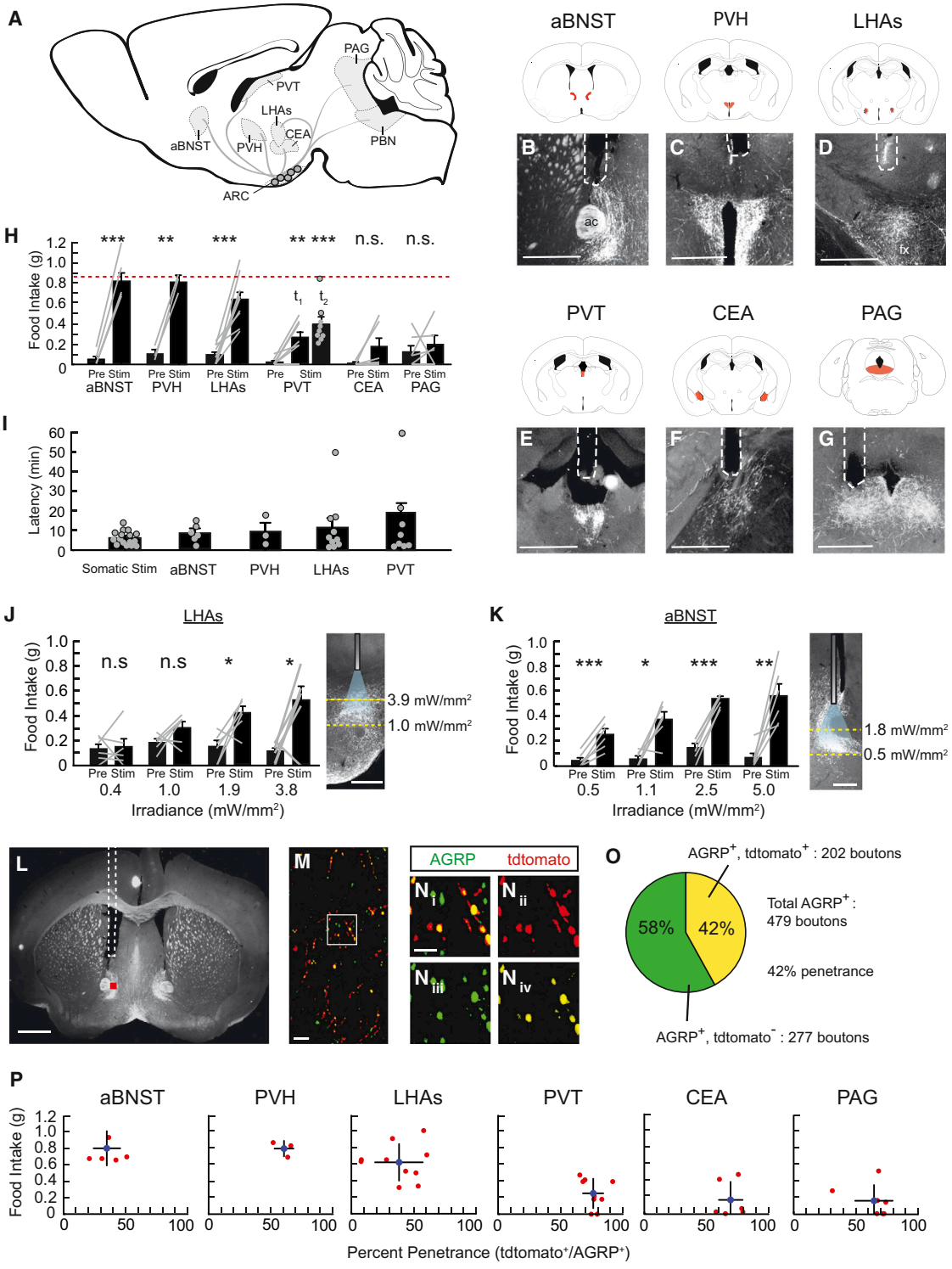

Figure 1. Evoked Food Intake from Activation of AGRP Neuron Axon Projections

(A) Diagram of prominent AGRP neuron axon projections analyzed in this study. Axon trajectories are schematic.

(B–G) Diagrams and images of ChR2tdtomato-expressing AGRP neuron axon projections and optical fiber placement (white dotted line). ac: anterior commissure. fx: fornix. Scale bar, 500 μm.

(H) Food intake before (pre) and during (stim) photostimulation of AGRP neuron axon projection fields. (PVH: n = 3, aBNST: n = 6, LHAs: n = 10, PVT: n = 9, CEA: n = 6, PAG: n = 7). Red dotted line: Mean food intake from somatic photostimulation (Aponte et al., 2011). For PVT experiments, data are shown from successive evoked feeding trials (t_1, t_2). Values are mean ± SEM. Paired t tests, n.s. $p > 0.05$, **$p < 0.01$, ***$p < 0.001$.

(legend continued on next page)

To gain insight into the coordination of feeding behavior, we systematically probed the functional and anatomical properties of AGRP neuron axon projections to intra- and extrahypothalamic sites. Projection-specific optogenetic stimulation of AGRP axon projections revealed multiple brain regions, not previously associated with acute feeding, that were sufficient to evoke avid food consumption. To understand the anatomical relationship between distinct AGRP neuron projection fields, we used a viral approach for cell-type-specific axon transduction to delineate the anatomy of the different projection fields. These experiments showed that each axon projection originated from a separate, distinct subpopulation of AGRP neurons. Therefore, AGRP neuron subpopulations form discrete, redundant, parallel circuits, and multiple populations projecting to different regions are each sufficient to control feeding behavior.

RESULTS

Axon Projections Reveal Brain Regions that Are Sufficient to Elicit Feeding

The axon projections of AGRP neurons reveal a blueprint of the downstream circuit elements that coordinate the complex behavioral responses for feeding (Sternson, 2013). To determine the functional influence of different AGRP neuron projections on food intake, we photoactivated prominent axon projection fields in *Agrp-IRES-Cre* mice that were engineered to express channelrhodopsin-2 (ChR2) using the Cre-dependent viral vector, AAV2/10rh-FLEX-*rev*-ChR2tdtomato (Atasoy et al., 2008). Light was delivered through implanted optical fibers targeted to intrahypothalamic projections: PVH and suprafornical subdivision of the lateral hypothalamic area (LHAs) (Hahn and Swanson, 2010); or extrahypothalamic projections: anterior subdivisions of the bed nucleus of the stria terminalis (aBNST), paraventricular thalamic nucleus (PVT), central nucleus of the amygdala (CEA), and periaqueductal gray (PAG) (Figures 1A–1G). These axon projections fill substantial portions of each region with axonal boutons, indicating that they are the targets of AGRP projections. Light-evoked feeding was observed with separate activation of only a subset of the projection fields: $ARC^{AGRP} \rightarrow$aBNST, $ARC^{AGRP} \rightarrow$PVH (as in Atasoy et al., 2012), $ARC^{AGRP} \rightarrow$LHAs, and $ARC^{AGRP} \rightarrow$PVT (Figure 1H). For these experiments, the latency to initiate the first bout of feeding was usually comparable to AGRP neuron somatic photostimulation (Figure 1I). Activation of other projection fields did not significantly increase feeding: $ARC^{AGRP} \rightarrow$CEA, $ARC^{AGRP} \rightarrow$PAG (Figure 1H); in addition, prior work showed that $ARC^{AGRP} \rightarrow$PBN (parabrachial nucleus) activation also did not elevate food consumption (Atasoy et al., 2012). Therefore, we find multiple AGRP axonal projection fields that are sufficient to evoke feeding similar to AGRP neuron somatic activation (PVH, aBNST, LHAs), or to a reduced degree (PVT), and others that are not (CEA, PAG, PBN).

Although photostimulation offers cell-type-specific control of axonal activation, both aBNST and LHAs are nearby regions containing AGRP axon projections, and light scattering could potentially result in activation of these neighboring axons. To address this possibility and improve the spatial specificity for axon activation, we titrated light intensity to the threshold for ChR2 activation (~50% activated at 1 mW/mm^2 [Lin et al., 2009]) in the vicinity of the projection field, based on a theoretical model (Aravanis et al., 2007) of light absorption and scattering in neural tissue (Figures 1J and 1K; see Extended Experimental Procedures). For $ARC^{AGRP} \rightarrow$LHAs, irradiance at the target region larger than 1 mW/mm^2 significantly elevated feeding, while light power densities below this level did not (Figure 1J). For $ARC^{AGRP} \rightarrow$aBNST, irradiance at the target region larger than 0.5 mW/mm^2 resulted in increased food intake (Figure 1K). These experiments further substantiate our finding that AGRP axons projecting to LHAs and aBNST are sufficient to evoke feeding.

Photostimulation of $ARC^{AGRP} \rightarrow$PVT projections significantly increased food consumption (Figure 1H), but the response magnitude was substantially lower than for somatic stimulation. Mean response latencies were longer than for somatic stimulation, but the difference was not statistically significant (Figure 1I, ANOVA $F(4,39) = 1.39$, $p = 0.26$). We also found that a subsequent trial with photostimulation of this projection showed increased reliability of food intake (Figure 1H), although this is not seen for other AGRP neuron projections (data not shown) or somatic activation (Aponte et al., 2011).

Because the magnitude of evoked food intake during AGRP neuron stimulation is dependent on the penetrance of ChR2 expression in virally transduced neurons (Aponte et al., 2011), we measured ChR2tdtomato transgene expression in each axon projection field that we stimulated. Transgene penetrance in axons was calculated as the fraction of AGRP-immunoreactive boutons coexpressing ChR2tdtomato in each projection field (Figures 1L–1O). We found that even unilateral photostimulation of AGRP axon projections to the aBNST, LHAs, or PVH evokes robust feeding with low penetrance ChR2 expression (Figure 1P). In contrast, $ARC^{AGRP} \rightarrow$PVT stimulation evoked only moderate levels of feeding with bilateral activation and high ChR2 penetrance (Figure 1P). Furthermore, photoactivation of $ARC^{AGRP} \rightarrow$PAG or $ARC^{AGRP} \rightarrow$CEA did not significantly elevate feeding even with high levels of ChR2tdtomato penetrance and bilateral stimulation (for CEA), suggesting that AGRP projections to these regions are not sufficient to independently evoke feeding under our conditions (Figure 1P). These

(I) Latency to initiate first bout of feeding after photostimulation onset. Latency data for somatic photostimulation from (Aponte et al., 2011). Values are mean ± SEM.

(J and K) Evoked feeding for axon projection photostimulation in the LHAs and aBNST for different irradiances (calculated for distal portion of target region). Images depict estimated irradiance values bracketing targeted projection fields based on theoretical model (Aravanis et al., 2007). Scale bar, 500 μm. Paired t tests. n.s. $p > 0.05$, *$p < 0.05$, **$p < 0.01$, ***$p < 0.001$. Values are mean ± SEM.

(L) Fiber placement and ChR2tdtomato distribution in $ARC^{AGRP} \rightarrow$aBNST axon projections. Red square: area imaged for transgene penetrance. Scale bar, 1 mm.

(M) Inset from (L) showing a confocal image of AGRP (green) and tdtomato immunofluorescence (red). Scale bar, 10 μm.

(N) Inset from (M) showing AGRP and tdtomato immunofluorescence in individual boutons. Scale bar, 5 μm.

(O) ChR2tdtomato penetrance for the aBNST in (L).

(P) Food intake as a function of ChR2tdtomato penetrance in each projection field. Red dots, individual animals. Blue dot, mean. Scale bars, SD.

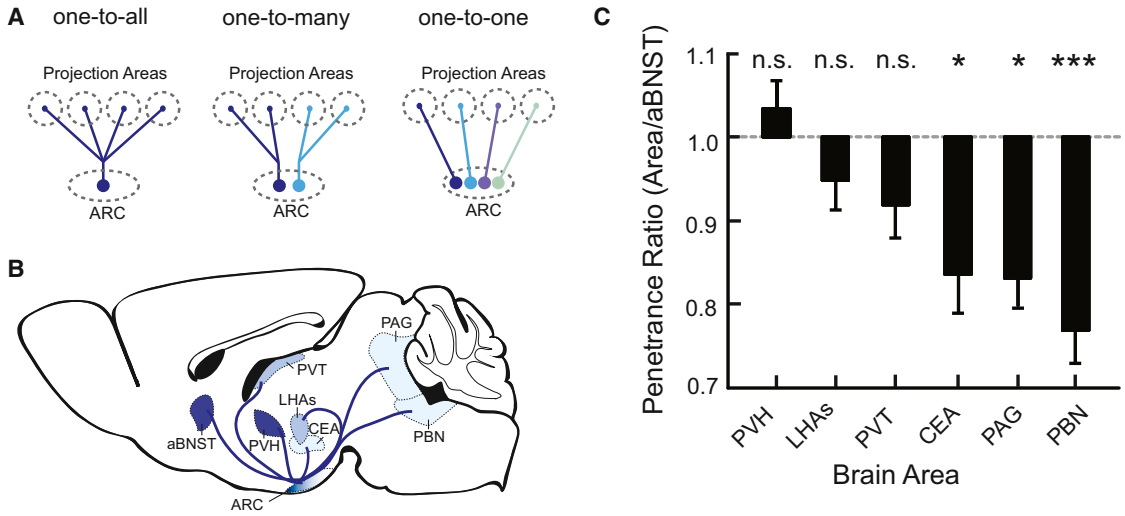

Figure 2. Inhomogeneous Transgene Penetrance in AGRP Neuron Axon Projections

(A) Potential configurations for AGRP neuron axon projections. Shading denotes hypothetical subpopulations.

(B) For one-to-many or one-to-one wiring configurations, fluorescent protein expression (blue) in a subset of AGRP neurons would be heterogeneously distributed. For one-to-all wiring, fluorescent protein expression in a subset of AGRP neurons would be evenly distributed to all projection fields.

(C) Fluorescent protein penetrance ratio with AGRP immunoreactivity, which is normalized to aBNST penetrance for each animal. Values are mean ± SEM. Paired t tests against unity ratio. Holm's correction for multiple comparisons.

experiments reveal a forebrain feeding circuit involving AGRP neuron projections to the aBNST, PVH, and LHAs, which exhibits similar characteristics in magnitude and latency to elicit food consumption. The $ARC^{AGRP} \rightarrow PVT$ projection appears capable of inducing feeding behavior, albeit with characteristics distinct from the other regions. AGRP neuron projections to the amygdala and the hindbrain were not sufficient to evoke feeding behavior.

Separate, Parallel Anatomical Configuration of AGRP Neuron Circuits

The heterogeneity of behavioral responses during stimulation of different AGRP neuron projection fields, which can be categorized as feeding sufficient or feeding insufficient, raises questions about their respective anatomical organization. We envisioned three configurations for AGRP neuron interactions with downstream brain regions (Figure 2A). Divergent, one-to-all connectivity would involve each AGRP neuron projecting to every target region through extensive axon collateralization. This configuration is well suited for simultaneous communication across diverse brain regions. For a one-to-many arrangement, groups of AGRP neurons project collateralized axons to subsets of target regions with related functions. Alternatively, in a one-to-one model, each projection field is a separate communication channel that originates from a group of neurons that do not send collateral projections to other target regions. Because little is known about the relationship of anatomical structure and function for neural circuits controlling complex survival behaviors, we investigated which of these different circuit configurations is used by AGRP neurons.

The one-to-all model appears incompatible with our findings that show different functional outcomes for different axon projections. Photoactivation of one axon projection would be expected to result, via a back-propagating action potential, in activation of the entire neuron, including any putative axon collaterals (Lima et al., 2009). We attempted to falsify this model with an anatomical analysis that was based on the assumption that each AGRP neuron projects to each target region. For the one-to-all model, expression of a fluorescent protein in a subset of AGRP neurons should result in similar transgene penetrance for each projection field. If the one-to-all configuration is false, then transgene penetrance levels would be heterogeneously distributed across projection fields (Figure 2B). After viral transduction targeting AGRP neurons in the anterior part of the ARC, we used aBNST penetrance as a reference and found that transgene penetrance was similar to the PVH, LHAs, and PVT axon projections (Figure 2C). In contrast, other brain regions showed penetrance significantly lower than the aBNST (Figure 2C). This analysis suggests that AGRP neurons are a heterogeneous population with subpopulations that project differently to separate brain regions, in contrast to the one-to-all model. However, these experiments do not allow us to distinguish between circuit configurations that involve collateralized axon projection groups (one-to-many) or noncollateralized one-to-one axonal connectivity.

To directly examine the anatomical organization of AGRP neurons and their connectivity with downstream brain regions, we implemented a strategy to virally transduce long-range axon projections. Axonal uptake of a viral vector and consequent expression of a fluorescent protein enables visualization of the entire neuron, including axon collaterals (Figures 3A). This approach is advantageous over traditional retrograde dye-labeling methods, which require a large number of multiplexed (usually pairwise) dye injections into each combination of a neuron

population's projection fields (Kuypers et al., 1977). To employ this strategy for cell type-selective, axon-selective neuron transduction, we used an envelope protein (EnvA) pseudotyped and rabies glycoprotein deleted rabies viral vector modified to express mCherry [SADΔG-mCherry(EnvA)] (Huang et al., 2013; Wickersham et al., 2007). AGRP neurons were engineered to coexpress the EnvA receptor, avian tumor virus receptor A (TVA), along with blue fluorescent protein (BFP) (Figures 3A and 3B). Thus, TVA-expressing axons originating from AGRP neurons were selectively competent for transduction by SADΔG-mCherry(EnvA) through targeted injections into discrete axon projection fields (Figure 3A). After rabies virus projection field infection, mCherry was expressed in a subset of ARC neurons (Figure 3C) and colocalized with BFP, demonstrating that AGRP neurons were transduced (Figure 3D). Although rabies virus is typically transported transsynaptically, the virus was engineered to lack the critical rabies glycoprotein G gene (RabiesG), thereby preventing transsynaptic spread. Axonally transduced AGRP neurons express high levels of mCherry, which allowed visualization of axon projections. For example, after SADΔG-mCherry(EnvA) injection into the PVH of $AGRP^{TVA/BFP}$-expressing mice, we find coexpression of BFP and mCherry in ARC^{AGRP} neurons, as well as colocalization of AGRP and mCherry in axonal boutons within the PVH (Figure 3E). Notably, other AGRP neuron projection sites showed very low or undetectable levels of mCherry expression (Figure 3E). This striking result indicates that $ARC^{AGRP} \rightarrow$ PVH projections lack prominent collateral axon projections, contrary to the one-to-all and one-to-many circuit models (Figure 3A).

To quantitatively evaluate potential axon collateralization of AGRP neurons transduced by SADΔG-mCherry(EnvA), we calculated the penetrance of mCherry colocalization with AGRP immunoreactivity at the injection site and compared this with mCherry penetrance at ten other projection sites. This analysis was performed on mouse brains that had been injected with SADΔG-mCherry(EnvA) in one of six target regions that contain prominent AGRP neuron projection fields: aBNST, PVH, PVT, CEA, PAG, PBN. At the SADΔG-mCherry(EnvA) injection site within a targeted AGRP neuron axon projection field, mCherry penetrance varied from 4%–27% (Figures 3F, 3J, and 3N). For regions outside the targeted injection site, mCherry was either not detected or exhibited much lower penetrance (Figures 3F–3O). These experiments indicate that AGRP neuron projections investigated here lack extensive collateral axon projections to other regions. However, we also noticed that regions proximal to the SADΔG-mCherry(EnvA) injection site sometimes showed a small degree of mCherry/AGRP colocalization in axonal boutons (Figures 3G, 3I, and 3O), raising the possibility that either some AGRP neurons send an axon collateral to nearby target regions, or, alternatively, SADΔG-mCherry injections may have diffused to infect axons of neighboring regions.

To examine whether AGRP neurons share axon collaterals with neighboring brain regions we used a genetic approach to localize the axonal viral transduction with transsynaptic retrograde rabies virus tracing from a single AGRP neuron target region (Figure 4A) (Wall et al., 2010). Because our analysis of $ARC^{AGRP} \rightarrow$ PVH projections showed the largest amount of mCherry/AGRP colocalization outside of the injection site, we focused on this projection. For transsynaptic labeling, PVH neurons were transduced with a precise injection of a tricistronic viral vector expressing BFP, TVA, and RabiesG (AAV2/1-FLEX-*rev*-BFP-2a-TVA-2a-RabiesG) in *Sim1-Cre* transgenic mice, which is a line that marks most PVH neurons (Figure 4B) (Balthasar et al., 2005). These "starter cells" were identified by BFP expression and overlapped the domain of $ARC^{AGRP} \rightarrow$ PVH neuron projections (Figure 4C). After SADΔG-mCherry(EnvA) transduction, these neurons expressed mCherry along with retrogradely labeled PVH^{SIM1}-projecting neurons (Figure 4D). In accord with established ARC → PVH synaptic connectivity (Atasoy et al., 2008; Atasoy et al., 2012; Diano et al., 1998), we observed extensive retrograde labeling of neurons in the ARC (Figure 4E). To identify the AGRP neurons in this retrogradely labeled group, we did not use AGRP immunoreactivity because it is distributed almost exclusively to axons. Instead, we developed a labeling strategy based on the intersection of immunoreactivity for the transcription factors FoxO1 and Islet1, which we found to reliably and solely mark AGRP neurons (Figure S1 available online). Inspecting the ARC for colocalization of these markers with mCherry, we determined that 180–300 AGRP neurons (n = 2 mice) were labeled with monosynaptic retrograde transduction from PVH^{SIM1} neurons (Figures 4F and 4F').

Precise transsynaptic retrograde labeling of an AGRP neuron subpopulation that projects to the PVH ($AGRP_{PVH}$ neurons), allowed us to assess putative collateral labeling in adjacent brain regions using AGRP and mCherry colocalization. We observed almost no colocalization of mCherry with AGRP boutons in regions outside the PVH, including nearby AGRP neuron projection fields. For example, the dense $ARC^{AGRP} \rightarrow$ Xi projection (Xi: Xiphoid nucleus, a small thalamic nucleus just dorsal to PVH) was nearly devoid of detectable mCherry fluorescence (1/894 AGRP boutons) with this labeling method in contrast to partial labeling in Xi that was observed when $ARC^{AGRP} \rightarrow$ PVH projections were targeted using the direct axon transduction approach (16/389 AGRP boutons) (Figure 3O). Similarly, scant AGRP/mCherry localization was observed in other nearby regions, including the LHAs (0/2,197 AGRP boutons), dorsomedial hypothalamic nucleus (DMH) (1/1,886 AGRP boutons), aBNST (1/4,638 AGRP boutons), and PVT (2/2,478 AGRP boutons). Negligible collateralization observed in $ARC^{AGRP} \rightarrow$ PVH projection neurons suggests labeling observed in nearby target regions by direct transduction of $AGRP^{TVA}$ axons (Figure 3) was likely due to spread of the SADΔG-mCherry(EnvA) following stereotaxic injection.

To further examine this striking lack of collateralization, we employed classical dual-color retrograde labeling methods (Kuypers et al., 1977). We first performed control experiments to assess the efficiency of retrograde transport of various reagents, which showed that coinjection of Fluoro-Gold (FG) and Red RetroBeads (RR) into an AGRP axon projection field resulted in extensive colocalization in ARC neurons (94% ± 8% colocalized, mean ± SD, n = 2 mice). Based on this efficient uptake and transport, we examined potential collateralization of neurons projecting to the aBNST and the PAG by targeted injections that filled these regions with either FG or RR beads. These regions were selected to represent axon projection fields that we found to be either feeding sufficient or feeding insufficient, respectively. Retrograde dye transport labeled AGRP neurons with

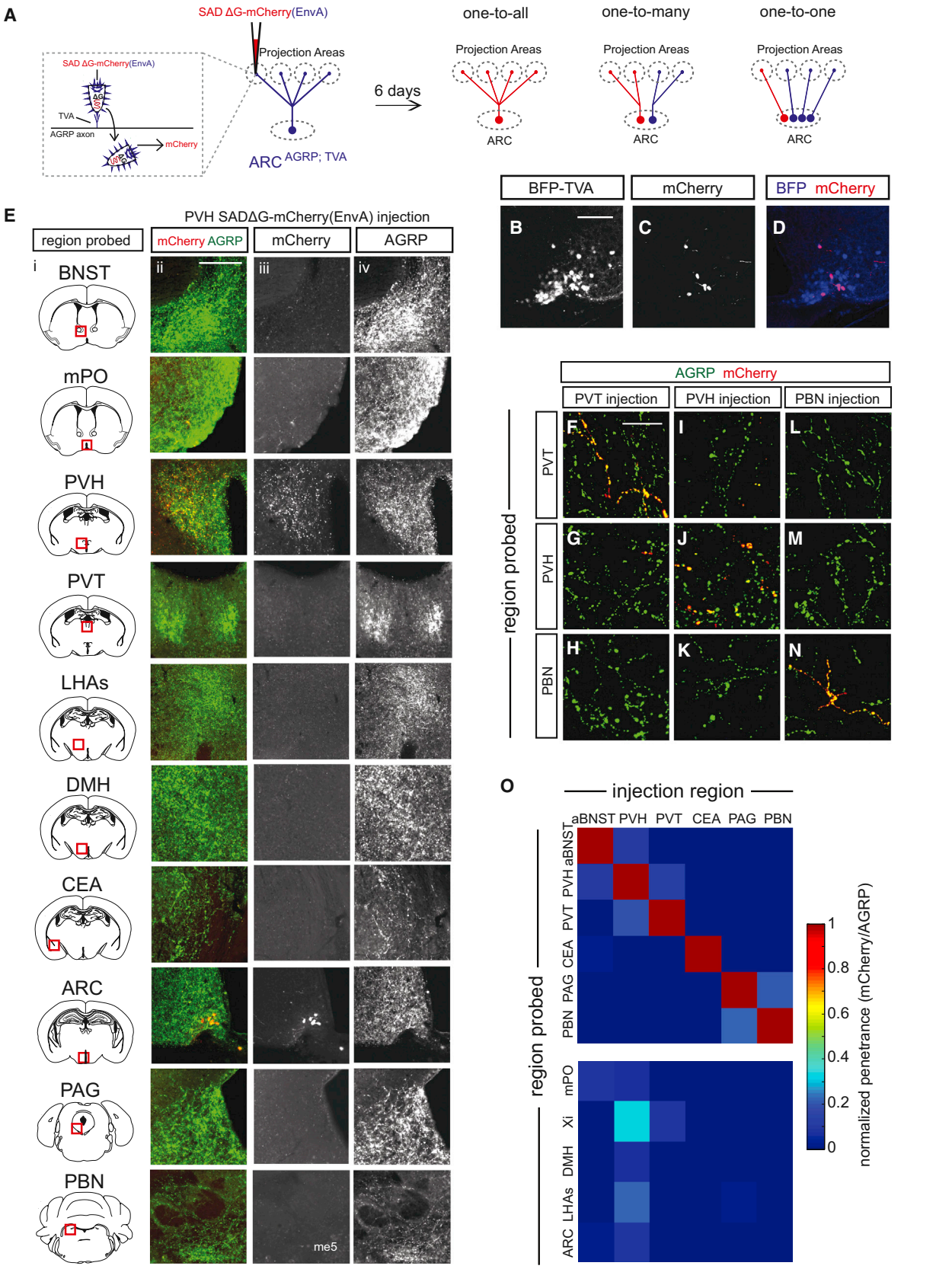

(legend on next page)

either FG or RR (10.8 ± 2.8 neurons/section, mean ± SD, n = 4 mice); however, colabeling was not observed in AGRP neurons (0/455 labeled neurons, n = 4 mice) (Figure 4G). Notably, a small number of non-AGRP ARC neurons (5/250) showed colabeling with retrograde transport from the BNST and the PAG (2.0% ± 0.6%, mean ± SD, n = 4 mice). Taken together, these experiments further support the conclusion that AGRP neurons use a one-to-one parallel circuit configuration in which neurons lack prominent collateral axons and are subdivided into distinct subpopulations that send projections to a single brain region. However, ARC neurons are not strictly prohibited from collateralization, and the wiring configuration is therefore a property of this particular cell type.

Quantitative Analysis of AGRP Neuron Projection Populations

Our results indicate that AGRP neurons can be subdivided into separate neuron subpopulations based on their projections. How many AGRP neurons are in each projection population? To determine this, we first measured the total number of AGRP neurons along the anterior-posterior axis of the ARC. We labeled all AGRP neurons by crossing *Agrp-IRES-Cre* to a Cre-dependent nuclear-GFP (nucGFP) reporter line. Although related approaches have permanently marked cells that transiently express Cre-recombinase (Padilla et al., 2010), we have determined that, using the *Agrp-IRES-Cre* mouse, this strategy labels only AGRP-expressing neurons (Figure S1). We find that the ARC contains 9,965 ± 66 AGRP neurons (mean ± SD, n = 2 mice), which are evenly distributed along the anterior to posterior ARC axis, except for drop-off at the boundaries (Figures 5A–5D).

Next, we calculated the number of AGRP neurons that project to each region by counting the mCherry-expressing neurons in the ARC from the brains that were axonally transduced by direct injection of SADΔG-mCherry(EnvA) in the aBNST, PVH, PVT, CEA, PAG, or PBN. The total number of neurons projecting to each region was estimated by normalizing these counts of retrogradely labeled AGRP neurons to the penetrance of mCherry in AGRP-containing boutons at each injection site. We find that the largest fraction of AGRP neurons project to the PVH ($AGRP_{PVH}$: 29.9% ± 7.4%) and the aBNST ($AGRP_{aBNST}$: 18.3% ± 3.3%) (Figure 5E). Target regions that do not evoke feeding with AGRP axonal activation are innervated by a much smaller percentage of AGRP neurons ($AGRP_{PAG}$: 4.0% ± 1.2%, $AGRP_{PBN}$: 3.1% ± 0.9%, $AGRP_{CEA}$: 2.2% ± 0.6%). The PVT, which evoked a moderate feeding response, is only innervated by 2.1% ± 0.2% of the AGRP neurons (Figure 5E). Our analysis accounts for 60% of AGRP neurons, but it does not include a number of intrahypothalamic projection populations that we could not selectively retrogradely label on account of their proximity to other axon projections. Future work with more precise viral delivery methods will be needed to accurately isolate these populations. We found that AGRP neuron subpopulations project to their target regions either ipsilaterally or contralaterally, but we do not find evidence of collateralized projections to both hemispheres (Figures 5G–5I). Moreover, we observed that neurons projecting to anterior brain regions are distributed in the anterior portion of the ARC, and those projecting to the hindbrain are distributed toward the posterior ARC (Figure 5F). This organization also explains the heterogeneous transgene distribution in penetrance analysis of anterior ARC viral injections from Figure 2C. Therefore, AGRP neuron projection populations have wide numerical differences in their representation within this molecularly defined population, and they are distributed topographically in the ARC based on their axon projection targets.

Homeostatic and Hormonal Regulation of AGRP Neuron Subpopulations

Our experiments indicate that AGRP neurons form separate projection populations, which have different capacities to evoke feeding behavior. This functional organization raises the prospect that distinct AGRP projection populations might be differentially regulated. To explore this possibility, we measured induction of the immediate early gene product Fos after food deprivation (24 hr) or the administration of ghrelin, a hormonal signal of energy deficit. We found that either food deprivation or ghrelin elevates Fos expression in most AGRP neurons but that the intensity of Fos immunoreactivity was variable (Figures 6A–6D and 6I). To see if distinct projection populations show different levels of Fos induction, we performed food deprivation or ghrelin administration in mice with FG microinjections to label $AGRP_{aBNST}$ or $AGRP_{PAG}$ neurons. These two neuron subpopulations are

Figure 3. Separate AGRP Neuron Subpopulations Project to Different Brain Regions

(A) Strategy and potential outcomes for cell-type-specific and axon-projection-specific neuron transduction to visualize potential axon collateral configurations for AGRP neurons. Cell-type-specific axon transduction with EnvA pseudotyped rabies virus requires the axonal expression of its receptor, TVA, for axonal uptake of the viral vector (inset) and fluorescent protein expression for neuron labeling.

(B) BFP fluorescence from AGRP neurons selectively transduced with AAV2/1-FLEX-*rev*-BFP-2a-TVA in an *Agrp-IRES-Cre* mouse. Scale bar, 100 μm.

(C) mCherry fluorescence in the ARC following SADΔG-mCherry(EnvA) injection to the PVH of a mouse expressing TVA in AGRP neurons.

(D) BFP and mCherry colocalization in AGRP neurons.

(E) Ten AGRP neuron projection fields probed for mCherry and AGRP expression following SADΔG-mCherry(EnvA) infection in the PVH of an $AGRP^{TVA}$ mouse. (i) Red box indicates region probed for axon collateralization of PVH-projecting AGRP neurons. (ii) Overlaid images of AGRP immunoreactivity and mCherry fluorescence. (iii) mCherry expression reveals axonal arborization in the injection site (PVH) but mCherry fluorescence was very low or undetectable in probed regions. (iv) AGRP immunofluorescence in each target region. mPO, medial preoptic area. DMH, dorsomedial hypothalamus. Mesencephalic trigeminal tract (me5) shows autofluorescence near the PBN. Scale bar, 200 μm.

(F–N) Representative confocal images of AGRP immunofluorescence and mCherry fluorescence in SADΔG-mCherry(EnvA) injection and probed sites. Scale bar, 20 μm.

(O) Penetrance of mCherry colocalization with AGRP-immunofluorescence in each region probed normalized to penetrance at the SADΔG-mCherry(EnvA) injection site. Colocalization was assessed in 1,510 ± 350 boutons per region (mean ± SD) (see Experimental Procedures and Extended Experimental Procedures). Xi, Xiphoid nucleus.

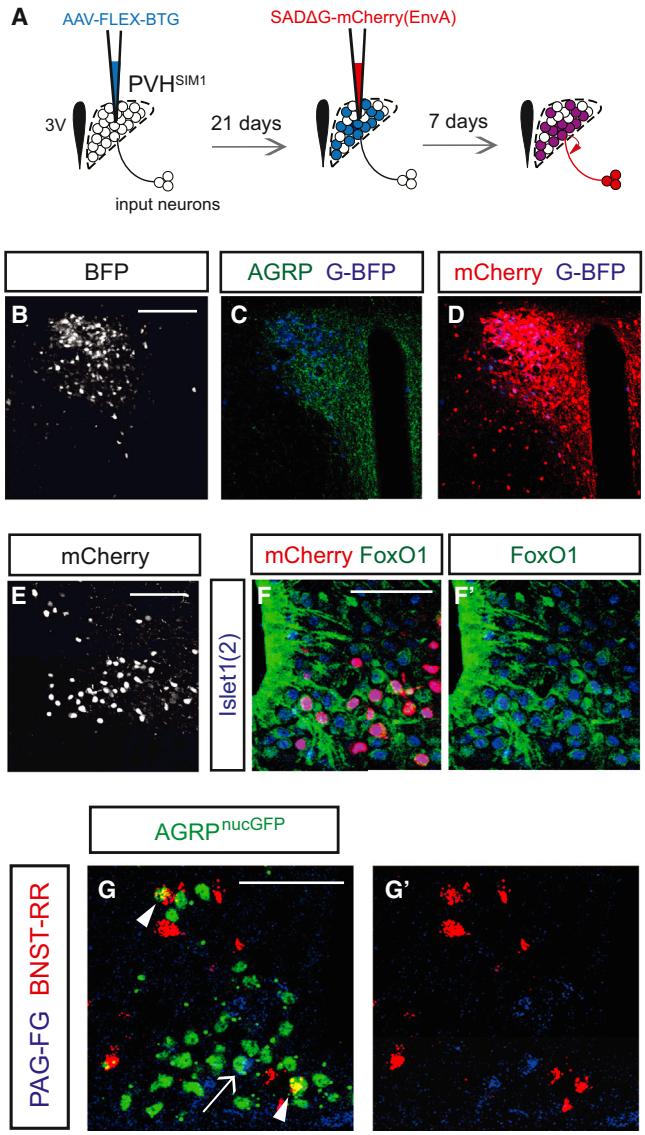

Figure 4. Transsynaptic Transduction of ARC^{AGRP}→PVH Projections Does Not Show Detectable Axon Collateralization

(A) Scheme for genetically targeting SADΔG-mCherry(EnvA) to the PVH for transsynaptic retrograde transduction of ARC^{AGRP}→PVH projections. AAV-FLEX-BTG: AAV2/1-FLEX-*rev*-BFP-2a-TVA-2a-RabiesG virus. Blue, BFP. Red, mCherry.

(B) Expression of BFP in PVH^{SIM1} neurons after viral transduction with AAV2/1-FLEX-*rev*-BFP-2a-TVA-2a-RabiesG virus in a *Sim1-Cre* transgenic mouse. Scale bar, 200 μm.

(C) Expression of BFP in PVH^{SIM1} neurons overlaps the domain of AGRP inputs to the PVH.

(D) PVH^{SIM1} starter cells coexpress BFP and mCherry following SADΔG-mCherry(EnvA) injection in the PVH.

(E) ARC neurons show retrograde labeling with mCherry after transsynaptic transduction from PVH neurons. Scale bar, 100 μm.

(F and F') AGRP neurons, identified by the coexpression of FoxO1 and Islet1(2), are a subset of mCherry retrogradely labeled ARC neurons. Scale bar, 50 μm.

(G and G') Retrograde transport of FluoroGold (FG) from the PAG and Red RetroBeads (RR) from the aBNST labels AGRP neurons in the ARC of *Agrp-IRES-Cre*;*ROSA::lox-STOP-lox-GNZ* mice that express nuclear GFP specifically in AGRP neurons (AGRP^{nucGFP}). Arrow identifies an AGRP^{nucGFP} neuron labeled with FG and arrowheads point to AGRP^{nucGFP} neurons labeled with RR. Scale bar, 100 μm.

See also Figure S1.

functionally distinguished by their capability or incapability, respectively, to evoke feeding behavior during selective activation of their axon projections. Nevertheless, both groups of neurons responded with similar heterogeneity of Fos intensity (Figures 6E–6H and 6J), and the cumulative probability distributions for Fos immunorectivity in these populations were not significantly different (Figure 6K, Dep: p = 0.75, Ghr: p = 0.13, Kolmogorov-Smirnov test), suggesting that these distinct neuron subpopulations are both sensitive to food deprivation and ghrelin.

The adipose-derived hormone, leptin, is another important peripheral signal of energy stores and is a negative regulator of AGRP neurons (van de Wall et al., 2008; van den Top et al., 2004), so we investigated leptin receptor expression in AGRP neuron projection populations. To visualize axon projections from neurons that express the leptin receptor, we used *Lepr-IRES-Cre* mice transduced in the ARC with AAV2/1-FLEX-*rev*-tdtomato. The distribution of leptin receptor-expressing, AGRP-containing axons was measured by the colocalization of axonal AGRP with tdtomato. We found that AGRP neurons with extrahypothalamic axonal projections were labeled by tdtomato, while intrahypothalamic AGRP neuron projections were not (Figures 6L–6O and 6T). These results indicate that, in AGRP neurons, direct leptin responsiveness is limited to extrahypothalamic AGRP neuron projection populations. In addition, this demonstrates that the parallel and redundant pathways through which AGRP neurons modulate feeding have the capacity to be differentially regulated.

For comparison, we also looked at the axon projections of neurons that express leptin receptor and Proopoiomelanocortin (POMC), which are intermingled with AGRP neurons in the ARC and have an important functional role for suppressing food consumption (Aponte et al., 2011; van de Wall et al., 2008). POMC neurons project to most of the same target regions as AGRP neurons. We find coexpression of leptin receptor in POMC neuron axon projections that target both intrahypothalamic and extrahypothalamic brain areas (Figures 6P–6S and 6T). This finding reveals asymmetry in the organization of projections from leptin-responsive AGRP and POMC neuron circuits.

Overall, these experiments show that AGRP neurons are comprised of multiple separate populations that form parallel output circuits to distinct brain regions, several of which can coordinate feeding behavior (Figure 6U). We have also found that these projection populations differ in abundance, are topographically organized in the ARC and show similar responses to signals of energy deficit but differential responses to leptin, a signal of energy surfeit (Figure 6U). Therefore, concerted functional and anatomical analysis of the separate axon projections from AGRP neurons reveals complex organization and regulation of this circumscribed, molecularly defined neuron population.

Relationship of AGRP Neuron Projections to PVH Inputs

Because some AGRP neuron circuits redundantly show the capacity to evoke feeding behavior but other circuit connections

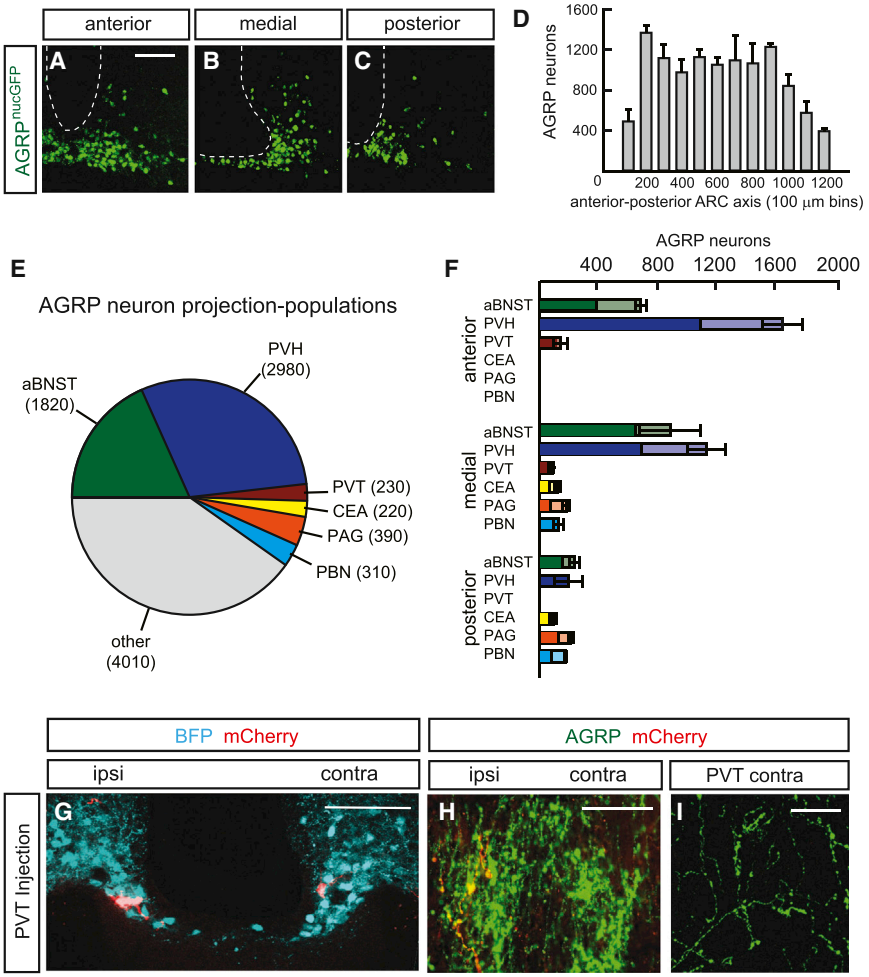

Figure 5. Size and Distribution of Separate AGRP Neuron Projection Populations

(A–C) Representative images of nuclear GFP in AGRP neurons along the anterior-posterior axis of the ARC. Scale bar, 100 μm.

(D) Distribution of AGRP neurons along the anterior-posterior axis of the ARC.

(E) Number of AGRP neurons estimated to comprise each projection population.

(F) Distribution of AGRP neuron projection populations along anterior-posterior axis of the ARC, subdivided into 400 μm bins. Shading denotes ipsilaterally (dark) and contralaterally (light) projecting subcomponents of each projection population. Values are mean ± SD, n = 2 mice.

(G–H) Bilateral labeling of ARC^{AGRP} neurons transduced by a unilateral injection of SADΔG-mCherry(EnvA) in the PVT (G). AGRP axons projecting to the PVT show mCherry fluorescence restricted ipsilateral to the injection site (H) (mCherry colocalization, ipsilateral: 320/2935 AGRP boutons, contralateral: 1/1010 AGRP boutons). Therefore, $AGRP_{PVT}$ neurons comprise separate ipsilateral or contralateral projecting subpopulations. Scale bar, 100 μm.

(I) AGRP-containing boutons lack mCherry fluorescence in the hemisphere contralateral to SADΔG-mCherry(EnvA) axonal infection in the PVT. Scale bar, 20 μm. See also Figure S1.

do not, we were also interested in whether regions targeted by feeding-insufficient AGRP neuron projections might be in a position to affect feeding by providing modulatory inputs to regions targeted by feeding-sufficient projections. To understand the potential connectivity between these two categories of projection fields, we analyzed the transsynaptic retrograde labeling of afferents to PVH^{SIM1} neurons (Figure 4A) for their overlap with AGRP neuron axon projections. Retrogradely labeled neurons from the PVH were found, with varying density, in all of the regions that receive AGRP neuron axonal input. AGRP neuron axon projections that were insufficient to evoke feeding (PBN, PAG, CEA) showed strong overlap with neurons projecting to the PVH (Figures 7A–7C). Brain regions innervated by AGRP projections that robustly evoked feeding (aBNST and LHAs) also exhibited retrograde labeling (Figures 7D and 7E). In addition, we observed retrograde labeling from PVH^{SIM1} neurons in the PVT, but this was mostly limited to a dorsal compartment of the PVT, while AGRP neuron projections were concentrated ventrally (Figure 7F). This anatomical arrangement highlights both the interconnectedness of brain areas that are sufficient to evoke feeding and also a feedforward circuit relationship by which AGRP neuron projections that are insufficient to evoke feeding might interact with the PVH (Figure 7K), a brain region that has been shown to elicit feeding behavior (Atasoy et al., 2012; Balthasar et al., 2005; Kelly et al., 1977).

Retrograde labeling of PVH^{SIM1} neurons also shows that PVH neurons receive inputs from cortical areas not contacted by AGRP neuron projections that possibly reflect circuits for emotional, volitional, or habitual control over feeding behavior. Neurons labeled from the PVH by retrograde transsynaptic transfer of rabies virus were found in the midcingulate cortex and insular cortex (Figures 7G and 7H). In addition, hippocampal inputs were observed from the ventral subiculum, along with the lateral septum (Figures 7I and 7J), which is a major target structure for region CA1 of the hippocampus (Swanson, 2000). The identification of cortical, hippocampal, and septal connections to the PVH, a brain region that is sufficient to bidirectionally regulate appetite (Atasoy et al., 2012), may reflect additional control points for feeding behavior.

DISCUSSION

Here, we systematically examined the anatomical and functional organization of AGRP neuron circuitry, a sensory system that responds to energy deficit. Axon-type-specific anatomical analysis revealed that the molecularly defined AGRP neuron population is comprised of separate projection populations, each targeting a specific brain region and hemisphere. The anatomical independence of these circuit connections validated the use of cell-type-specific axon activation techniques to show

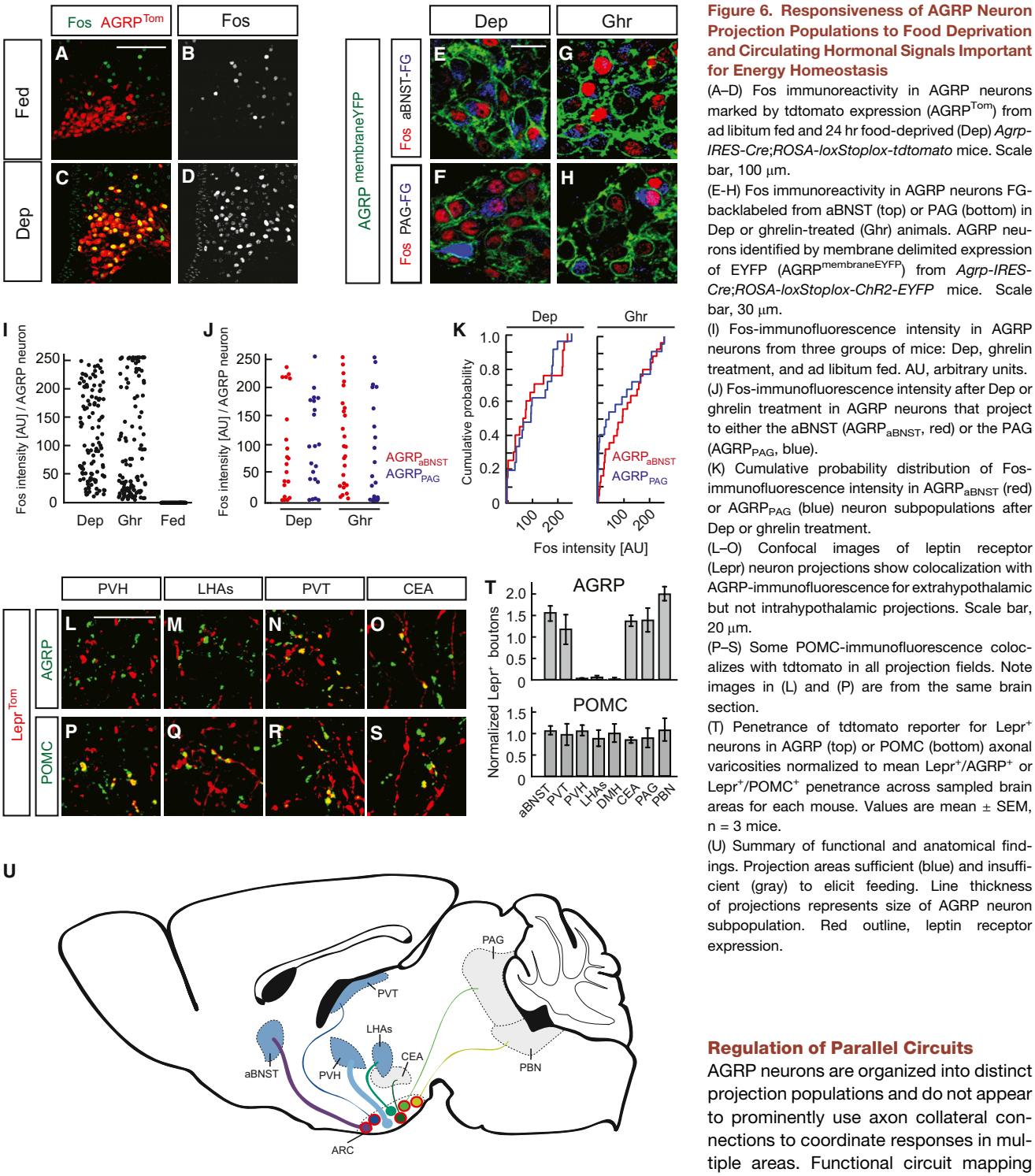

Figure 6. Responsiveness of AGRP Neuron Projection Populations to Food Deprivation and Circulating Hormonal Signals Important for Energy Homeostasis

(A–D) Fos immunoreactivity in AGRP neurons marked by tdtomato expression ($AGRP^{Tom}$) from ad libitum fed and 24 hr food-deprived (Dep) *Agrp-IRES-Cre;ROSA-loxStoplox-tdtomato* mice. Scale bar, 100 μm.

(E-H) Fos immunoreactivity in AGRP neurons FG-backlabeled from aBNST (top) or PAG (bottom) in Dep or ghrelin-treated (Ghr) animals. AGRP neurons identified by membrane delimited expression of EYFP ($AGRP^{membraneEYFP}$) from *Agrp-IRES-Cre;ROSA-loxStoplox-ChR2-EYFP* mice. Scale bar, 30 μm.

(I) Fos-immunofluorescence intensity in AGRP neurons from three groups of mice: Dep, ghrelin treatment, and ad libitum fed. AU, arbitrary units.

(J) Fos-immunofluorescence intensity after Dep or ghrelin treatment in AGRP neurons that project to either the aBNST ($AGRP_{aBNST}$, red) or the PAG ($AGRP_{PAG}$, blue).

(K) Cumulative probability distribution of Fos-immunofluorescence intensity in $AGRP_{aBNST}$ (red) or $AGRP_{PAG}$ (blue) neuron subpopulations after Dep or ghrelin treatment.

(L–O) Confocal images of leptin receptor (Lepr) neuron projections show colocalization with AGRP-immunofluorescence for extrahypothalamic but not intrahypothalamic projections. Scale bar, 20 μm.

(P–S) Some POMC-immunofluorescence colocalizes with tdtomato in all projection fields. Note images in (L) and (P) are from the same brain section.

(T) Penetrance of tdtomato reporter for $Lepr^+$ neurons in AGRP (top) or POMC (bottom) axonal varicosities normalized to mean $Lepr^+/AGRP^+$ or $Lepr^+/POMC^+$ penetrance across sampled brain areas for each mouse. Values are mean ± SEM, n = 3 mice.

(U) Summary of functional and anatomical findings. Projection areas sufficient (blue) and insufficient (gray) to elicit feeding. Line thickness of projections represents size of AGRP neuron subpopulation. Red outline, leptin receptor expression.

that AGRP neurons can elicit feeding behavior through projections to four separate forebrain regions: aBNST, PVH, LHAs, and PVT. Therefore, this survival circuit is configured with distinct parallel circuit elements, some of which have a redundant capability to drive feeding behavior.

Regulation of Parallel Circuits

AGRP neurons are organized into distinct projection populations and do not appear to prominently use axon collateral connections to coordinate responses in multiple areas. Functional circuit mapping experiments indicate that AGRP neurons are not synaptically interconnected (Atasoy et al., 2012). However, we did identify a small proportion of non-AGRP ARC neurons with dual retrograde dye labeling that projected to both the BNST and PAG. Moreover, a low rate of ARC neuron collateralization has been reported previously in the rat (Chronwall, 1985). Lack of detectable AGRP neuron

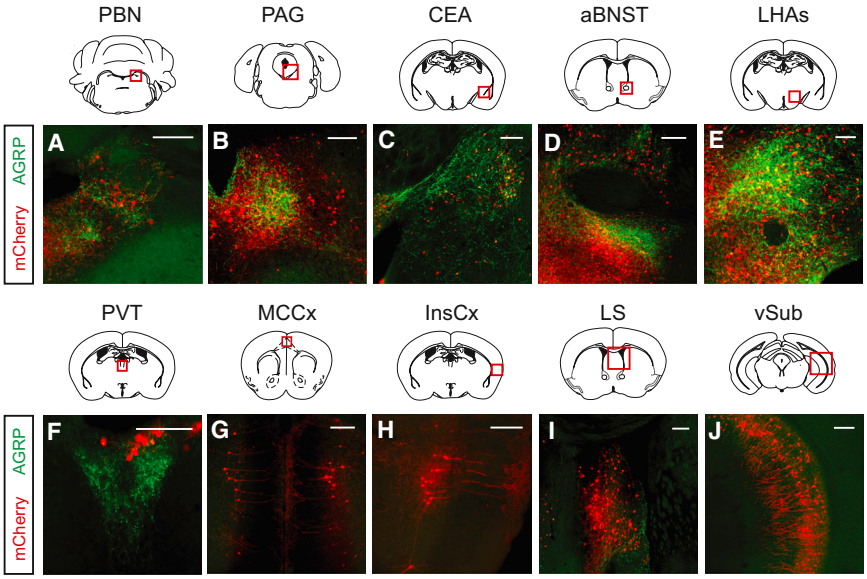

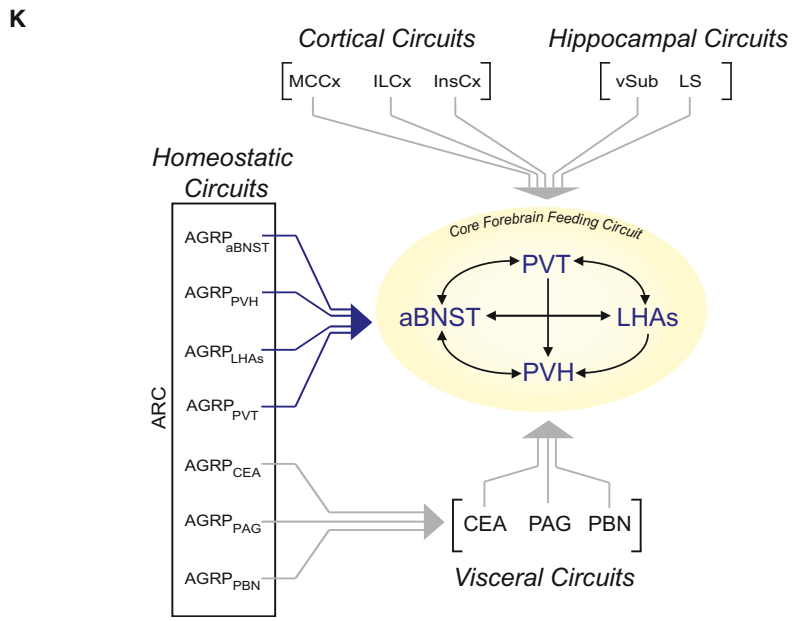

Figure 7. Core and Extended Feeding Circuits

(A–J) Neurons retrogradely labeled from PVH^{SIM1} neurons (mCherry fluorescence, red) in relation to prominent AGRP neuron axon projection fields (A–F) (AGRP immunoreactivity, green) and higher-order brain regions (G–J). Midcingulate cortex (MCCx) Insular cortex (InsCx), ventral Subiculum (vSub), Lateral septum (LS). Scale bar, 200 μm.

(K) A core feeding circuit comprised of interconnections between PVH, aBNST, LHAs, and PVT brain areas. The core feeding circuit is modulated by multiple inputs including homeostatic inputs, for example from AGRP neurons; cortical and hippocampal areas; as well as visceral processing areas. Homeostatic AGRP neuron projections also modulate the inputs to the core feeding circuit, such as the visceral processing areas. Blue arrows: projections sufficient to evoke eating. ILCx, Infralimbic cortex.

axon collateralization suggests that this property is not a constraint of brain wiring in the hypothalamus and may have functional importance for the counter-regulatory response to energy deficit.

Distinct AGRP neuron projection populations appear to have both common and differing modes of hormonal and energetic state regulation. For AGRP neuron activation, which was probed by Fos induction, regulation by ghrelin or food deprivation appears similar in anatomically and functionally separate subpopulations. We also note that synaptic regulation can be consistent across most AGRP neurons, based on previous work showing that ghrelin-mediated upregulation of synaptic activity to AGRP neurons (Yang et al., 2011) was observed for nearly all cells examined (7/8 neurons). Thus, separate populations of AGRP neurons can be similarly regulated by homeostatic, hormonal, or synaptic inputs.

In contrast, only AGRP neuron projection populations that project outside of the hypothalamus appear to express the receptor for the hormone leptin. The proportion of extrahypothalamic projecting AGRP neurons (~30%) is consistent with previous reports of leptin-mediated STAT3 phosphorylation in AGRP neurons (~35%) (van de Wall et al., 2008). Differential expression of leptin receptor in AGRP neuron projection populations may explain conflicting reports about leptin responsiveness in AGRP neurons (Claret et al., 2007; van den Top et al., 2004). Together, our experiments show that distinct AGRP neuron projection classes are regulated similarly by some hormonal signals and differently by others, indicating a previously unappreciated intricacy of physiological and neural control over anatomically distinct but behaviorally related AGRP neuron circuit projections.

Forebrain Regions that Control Feeding

The axon projections of AGRP neurons to the aBNST, LHAs, and PVT reveal brain regions with a capacity to orchestrate feeding behavior. In addition, prior work showed that ARC^{AGRP} → PVH projections evoke feeding (Atasoy et al., 2012). Most of the brain regions targeted by AGRP neuron projections have been only lightly characterized for their influence on feeding behavior, therefore following the axon projections of this interoceptive population helps identify brain areas sufficient to coordinate feeding behavior.

The BNST has been implicated in a broad range of behavioral roles including stress, addiction, reproduction, and defensive behavior, as well as neuroendocrine and autonomic functions. Based on the selective anatomical connectivity of ARC^{AGRP}→aBNST axons, the aBNST is shown here to have functional properties that are sufficient to rapidly orchestrate feeding behavior.

The lateral hypothalamus is a loosely defined brain region that is associated with multiple behavioral and autonomic outputs. The LHAs is a subdivision of the lateral hypothalamus that receives robust AGRP neuron input. Our anatomical analysis did not directly isolate the ARC^{AGRP}→LHAs projection because we could not restrict rabies virus injection solely to this domain. However, none of the other sites that we targeted for anatomical analysis, including the nearby PVH, showed collateral AGRP axon projections to the LHAs. Therefore, it is likely that this projection is also anatomically distinct and that ARC^{AGRP}→LHAs photostimulation engages this specific suprafornical LHA subdomain for the control of feeding behavior.

The PVT is an integratory area and GABA-A receptor agonist microinjections (Stratford and Wirtshafter, 2013) are reported to increase food consumption. In our experiments, activation of ARC^{AGRP}→PVT projections, which release GABA (Atasoy et al., 2012), significantly increased food intake, but consumption was lower than for other projection fields.

Interconnected Second-Order Nodes Define a Core Feeding Circuit

A major implication of our systematic examination of AGRP neuron projections is that they point to a core feeding circuit involving the aBNST, PVH, LHAs, and to a lesser extent the PVT (Figure 6U). The capability of multiple, independent projections to separately evoke a complex behavioral response such as feeding suggests that these second-order circuit elements are likely functionally interconnected (Figure 7K).

The PVH is an integratory center for coordination of appetite (Swanson, 2000), and multiple brain regions targeted by AGRP neurons might act through the PVH. Indeed, the PVH receives inputs from each of the brain areas targeted by AGRP neuron axons. However, the PVH is unlikely to be the sole convergence point for these feeding circuits. Pharmacological blockade of ARC^{AGRP}→PVH connections during AGRP neuron activation suppressed food intake by only ~50% (Atasoy et al., 2012). This pharmacological manipulation likely also disrupts the overall function of the PVH, including afferent inputs from the aBNST and LHAs. Based on the AGRP neuron projection stimulation experiments here, this suggests that feeding can also be separately coordinated by the aBNST and/or the LHAs when ARC^{AGRP}→PVH is blocked.

Retrograde and anterograde anatomical studies report strong bidirectional connectivity between aBNST and LHAs (Hahn and Swanson, 2010; Shin et al., 2008), indicating a circuit involving these two brain areas that are targeted by AGRP neurons. The aBNST, but not the LHAs, is also reported to receive input from the PVH (Wittmann et al., 2009). In addition, the PVT is bidirectionally connected with both the aBNST and the LHAs (Hahn and Swanson, 2010; Shin et al., 2008). Taken together, the independent projections from AGRP neuron subpopulations highlight a core set of interconnected brain regions that are sufficient to evoke feeding (Figure 7K).

This core forebrain feeding circuit is positioned to participate in an extended circuit that can be modulated by multiple inputs from: (1) homeostatic circuits that signal survival needs, (2) visceral circuits that reflect organ states (such as fullness of the stomach or nausea), and (3) higher-order cortical circuits that may be involved in flexible control over feeding. Direct neocortical inputs to the core feeding circuit are from the infralimbic, midcingulate, and insular cortices. We found that the PVH receives input from the midcingulate cortex, a region associated with the experience of negative visceral states (Napadow et al., 2013). The aBNST and the LHAs receive input from the infralimbic cortex (Hahn and Swanson, 2010; Shin et al., 2008). The aBNST (Shin et al., 2008), LHAs (Hahn and Swanson, 2010), and PVH (Figure 7H) receive input from the insular cortex, which is associated with visceral sensation. Hippocampal circuits are also in a position to exert control over the core feeding circuit. Direct hippocampal input to the PVH was found from the ventral subiculum (Figure 7J), which is a brain structure important for control of emotional processes (Fanselow and Dong, 2010; Swanson, 2000). Hippocampal control is also mediated via input to the lateral septum, which projects to neurons in the PVH (Figure 7I) and to the aBNST (Risold et al., 1997; Shin et al., 2008). Through cortical connectivity, this core feeding circuit can be influenced by higher-order brain regions, which may represent pathways that extend beyond basic homeostatic regulation, for example cognitive and emotional control.

A number of AGRP neuron projection fields to brain regions associated with visceral processing were not sufficient to evoke feeding (ARC^{AGRP}→CEA, ARC^{AGRP}→PAG, ARC^{AGRP}→PBN). These projections may influence other aspects of AGRP neuron function, such as energy expenditure (Krashes et al., 2011) and fertility (Wu et al., 2012b). However, these brain areas also showed second-order interactions with the core feeding circuit nodes. Analysis of transsynaptic retrograde rabies virus tracing revealed that these AGRP neuron projection fields overlapped neurons that projected to PVH^{SIM1} neurons (Figures 7A–7C). In addition, experiments with retrogradely transported dyes indicated that each of these regions also project to aBNST and LHAs (Hahn and Swanson, 2010; Shin et al., 2008). These brain areas are involved in processing visceral information, and, in response to particular bodily or physiological stimuli, they may influence feeding behavior by interactions with this core feeding circuit in a manner subject to modulation by AGRP neurons. For example, PBN neurons communicate visceral information that appears to suppress feeding when AGRP input is lost (Wu et al., 2012a). Therefore, in addition to a core circuit, AGRP neuron projections may reveal key modulatory circuit nodes that are gated or otherwise regulated by AGRP neuron projections.

CONCLUSION

In this study, identification of multiple, distinct circuit projections, each with the capacity to evoke food consumption, provides a different view of feeding circuits than was previously apparent from studies of individual brain regions that influence appetite. The anatomical independence of AGRP axon projections points to a core feeding circuit that may serve as an interaction hub for

multiple different cortical, visceral, and homeostatic modulatory inputs that lead to appetite regulation.

The output connectivity of the core feeding circuit nodes is a key area for future investigation. The PVH, aBNST, LHAs, and PVT project to a number of motivationally important thalamic, midbrain, and hindbrain nuclei. One consideration for future examination of feeding behavior will be to focus on convergence points for the downstream projections of the PVH, aBNST, LHAs, and PVT. New tools for circuit tracing should enable experiments to identify convergence nodes that may provide insight to longstanding questions about how simple activity patterns in hypothalamic circuits selectively give rise to complex behavioral responses.

EXPERIMENTAL PROCEDURES

Experimental protocols were conducted according to U.S. National Institutes of Health guidelines for animal research and were approved by the Institutional Animal Care and Use Committee at Janelia Farm Research Campus.

Fluorescent Protein Penetrance in Virally Transduced Neurons

For transgene penetrance in AGRP neuron projection fields, we calculated colocalization of the transgene fluorescent protein reporter with AGRP immunoreactivity. For calculation of penetrance of reporter expression in *Agrp-IRES-Cre* mice (Figure 2), SADΔG-mCherry(EnvA) axonal (Figures 3 and 5) and retrograde transductions (Figure 4), and *Lepr-IRES-Cre* mice reporting tdtomato (Figure 6) at least 20 confocal images of AGRP boutons along the anterior-posterior axis of each target region were collected.

Statistics

Values are represented as mean ± SEM in figures and as mean ± SD in the text unless otherwise noted. Pairwise comparisons were calculated by unpaired or paired two-tail Student's t test. p values for comparisons across more than two groups were calculated using ANOVA. Post hoc multiple comparisons corrected using Holm's method. Kolmogorov-Smirnov test was used to compare distributions. Statistics were analyzed using SigmaPlot or Matlab. n.s. $p > 0.05$, *$p < 0.05$, **$p < 0.01$, ***$p < 0.001$.

SUPPLEMENTAL INFORMATION

Supplemental Information includes Extended Experimental Procedures and one figure and can be found with this article online at http://dx.doi.org/10.1016/j.cell.2013.11.002.

AUTHOR CONTRIBUTIONS

J.N.B., Z.F.H.C, and S.M.S designed the experiments and wrote the paper; J.N.B. performed anatomical analyses and behavior pilot studies; Z.F.H.C. performed behavioral experiments; and K.D.R. provided viral reagents.

ACKNOWLEDGMENTS

This research was funded by the Howard Hughes Medical Institute. Z.F.H.C. was funded by the HHMI Janelia Farm Graduate Scholar program. We thank A. Wardlaw, K. Morris, and J. Rouchard for mouse breeding, genotyping, and viral injections; M. Copeland for histology; S. Supekar and E. Betley for executing automated bouton counting; S. Brenner-Morton and T. Jessell for Islet1(2) antibody; M. Myers for *Lepr-IRES-Cre* mice; E. Callaway for rabies viral reagents.

Received: September 9, 2013
Revised: October 5, 2013
Accepted: October 8, 2013
Published: December 5, 2013

REFERENCES

Aponte, Y., Atasoy, D., and Sternson, S.M. (2011). AGRP neurons are sufficient to orchestrate feeding behavior rapidly and without training. Nat. Neurosci. *14*, 351–355.

Aravanis, A.M., Wang, L.P., Zhang, F., Meltzer, L.A., Mogri, M.Z., Schneider, M.B., and Deisseroth, K. (2007). An optical neural interface: in vivo control of rodent motor cortex with integrated fiberoptic and optogenetic technology. J. Neural Eng. *4*, S143–S156.

Atasoy, D., Aponte, Y., Su, H.H., and Sternson, S.M. (2008). A FLEX switch targets Channelrhodopsin-2 to multiple cell types for imaging and long-range circuit mapping. J. Neurosci. *28*, 7025–7030.

Atasoy, D., Betley, J.N., Su, H.H., and Sternson, S.M. (2012). Deconstruction of a neural circuit for hunger. Nature *488*, 172–177.

Balthasar, N., Dalgaard, L.T., Lee, C.E., Yu, J., Funahashi, H., Williams, T., Ferreira, M., Tang, V., McGovern, R.A., Kenny, C.D., et al. (2005). Divergence of melanocortin pathways in the control of food intake and energy expenditure. Cell *123*, 493–505.

Belgardt, B.F., Okamura, T., and Brüning, J.C. (2009). Hormone and glucose signalling in POMC and AgRP neurons. J. Physiol. *587*, 5305–5314.

Chronwall, B.M. (1985). Anatomy and physiology of the neuroendocrine arcuate nucleus. Peptides *6* (*Suppl 2*), 1–11.

Claret, M., Smith, M.A., Batterham, R.L., Selman, C., Choudhury, A.I., Fryer, L.G., Clements, M., Al-Qassab, H., Heffron, H., Xu, A.W., et al. (2007). AMPK is essential for energy homeostasis regulation and glucose sensing by POMC and AgRP neurons. J. Clin. Invest. *117*, 2325–2336.

Delgado, J.M., and Anand, B.K. (1953). Increase of food intake induced by electrical stimulation of the lateral hypothalamus. Am. J. Physiol. *172*, 162–168.

Diano, S., Naftolin, F., Goglia, F., Csernus, V., and Horvath, T.L. (1998). Monosynaptic pathway between the arcuate nucleus expressing glial type II iodothyronine 5′-deiodinase mRNA and the median eminence-projective TRH cells of the rat paraventricular nucleus. J. Neuroendocrinol. *10*, 731–742.

Fanselow, M.S., and Dong, H.W. (2010). Are the dorsal and ventral hippocampus functionally distinct structures? Neuron *65*, 7–19.

Hahn, J.D., and Swanson, L.W. (2010). Distinct patterns of neuronal inputs and outputs of the juxtaparaventricular and suprafornical regions of the lateral hypothalamic area in the male rat. Brain Res. Brain Res. Rev. *64*, 14–103.

Hess, W.R. (1957). The functional organization of the diencephalon (New York: Grune & Stratton).

Huang, C.-C., Sugino, K., Shima, Y., Guo, C., Bai, S., Mensh, B.D., Nelson, S.B., and Hantman, A.W. (2013). Convergence of pontine and proprioceptive streams onto multimodal cerebellar granule cells. Elife *2*, e00400.

Kelly, J., Alheid, G.F., Newberg, A., and Grossman, S.P. (1977). GABA stimulation and blockade in the hypothalamus and midbrain: effects on feeding and locomotor activity. Pharmacol. Biochem. Behav. *7*, 537–541.

Kirchgessner, A.L., and Sclafani, A. (1988). PVN-hindbrain pathway involved in the hypothalamic hyperphagia-obesity syndrome. Physiol. Behav. *42*, 517–528.

Kow, L.M., Montgomery, M.O., and Pfaff, D.W. (1977). Effects of spinal cord transections on lordosis reflex in female rats. Brain Res. *123*, 75–88.

Krashes, M.J., Koda, S., Ye, C., Rogan, S.C., Adams, A.C., Cusher, D.S., Maratos-Flier, E., Roth, B.L., and Lowell, B.B. (2011). Rapid, reversible activation of AgRP neurons drives feeding behavior in mice. J. Clin. Invest. *121*, 1424–1428.

Kruk, M.R., Van der Poel, A.M., Meelis, W., Hermans, J., Mostert, P.G., Mos, J., and Lohman, A.H. (1983). Discriminant analysis of the localization of aggression-inducing electrode placements in the hypothalamus of male rats. Brain Res. *260*, 61–79.

Kuypers, H.G., Catsman-Berrevoets, C.E., and Padt, R.E. (1977). Retrograde anoxal transport of fluorescent substances in the rat's forebrain. Neurosci. Lett. *6*, 127–133.

Lima, S.Q., Hromádka, T., Znamenskiy, P., and Zador, A.M. (2009). PINP: a new method of tagging neuronal populations for identification during in vivo electrophysiological recording. PLoS ONE *4*, e6099.

Lin, J.Y., Lin, M.Z., Steinbach, P., and Tsien, R.Y. (2009). Characterization of engineered channelrhodopsin variants with improved properties and kinetics. Biophys. J. *96*, 1803–1814.

Luquet, S., Perez, F.A., Hnasko, T.S., and Palmiter, R.D. (2005). NPY/AgRP neurons are essential for feeding in adult mice but can be ablated in neonates. Science *310*, 683–685.

Napadow, V., Sheehan, J.D., Kim, J., Lacount, L.T., Park, K., Kaptchuk, T.J., Rosen, B.R., and Kuo, B. (2013). The brain circuitry underlying the temporal evolution of nausea in humans. Cereb. Cortex *23*, 806–813.

Padilla, S.L., Carmody, J.S., and Zeltser, L.M. (2010). Pomc-expressing progenitors give rise to antagonistic neuronal populations in hypothalamic feeding circuits. Nat. Med. *16*, 403–405.

Risold, P.Y., Thompson, R.H., and Swanson, L.W. (1997). The structural organization of connections between hypothalamus and cerebral cortex. Brain Res. Brain Res. Rev. *24*, 197–254.

Roeling, T.A., Veening, J.G., Kruk, M.R., Peters, J.P., Vermelis, M.E., and Nieuwenhuys, R. (1994). Efferent connections of the hypothalamic "aggression area" in the rat. Neuroscience *59*, 1001–1024.

Shin, J.W., Geerling, J.C., and Loewy, A.D. (2008). Inputs to the ventrolateral bed nucleus of the stria terminalis. J. Comp. Neurol. *511*, 628–657.

Sternson, S.M. (2013). Hypothalamic survival circuits: blueprints for purposive behaviors. Neuron *77*, 810–824.

Stockinger, P., Kvitsiani, D., Rotkopf, S., Tirián, L., and Dickson, B.J. (2005). Neural circuitry that governs Drosophila male courtship behavior. Cell *121*, 795–807.

Stratford, T.R., and Wirtshafter, D. (2013). Injections of muscimol into the paraventricular thalamic nucleus, but not mediodorsal thalamic nuclei, induce feeding in rats. Brain Res. *1490*, 128–133.

Swanson, L.W. (2000). Cerebral hemisphere regulation of motivated behavior. Brain Res. *886*, 113–164.

Tinbergen, N. (1989). The Study of Instinct (New York: Oxford University Press).

van de Wall, E., Leshan, R., Xu, A.W., Balthasar, N., Coppari, R., Liu, S.M., Jo, Y.H., MacKenzie, R.G., Allison, D.B., Dun, N.J., et al. (2008). Collective and individual functions of leptin receptor modulated neurons controlling metabolism and ingestion. Endocrinology *149*, 1773–1785.

van den Top, M., Lee, K., Whyment, A.D., Blanks, A.M., and Spanswick, D. (2004). Orexigen-sensitive NPY/AgRP pacemaker neurons in the hypothalamic arcuate nucleus. Nat. Neurosci. *7*, 493–494.

Wall, N.R., Wickersham, I.R., Cetin, A., De La Parra, M., and Callaway, E.M. (2010). Monosynaptic circuit tracing in vivo through Cre-dependent targeting and complementation of modified rabies virus. Proc. Natl. Acad. Sci. USA *107*, 21848–21853.

Wickersham, I.R., Lyon, D.C., Barnard, R.J., Mori, T., Finke, S., Conzelmann, K.K., Young, J.A., and Callaway, E.M. (2007). Monosynaptic restriction of transsynaptic tracing from single, genetically targeted neurons. Neuron *53*, 639–647.

Wittmann, G., Füzesi, T., Singru, P.S., Liposits, Z., Lechan, R.M., and Fekete, C. (2009). Efferent projections of thyrotropin-releasing hormone-synthesizing neurons residing in the anterior parvocellular subdivision of the hypothalamic paraventricular nucleus. J. Comp. Neurol. *515*, 313–330.

Wu, Q., Clark, M.S., and Palmiter, R.D. (2012a). Deciphering a neuronal circuit that mediates appetite. Nature *483*, 594–597.

Wu, Q., Whiddon, B.B., and Palmiter, R.D. (2012b). Ablation of neurons expressing agouti-related protein, but not melanin concentrating hormone, in leptin-deficient mice restores metabolic functions and fertility. Proc. Natl. Acad. Sci. USA *109*, 3155–3160.

Yang, Y., Atasoy, D., Su, H.H., and Sternson, S.M. (2011). Hunger states switch a flip-flop memory circuit via a synaptic AMPK-dependent positive feedback loop. Cell *146*, 992–1003.

Note Added in Proof

While this manuscript was under review, activation of inhibitory neurons in the BNST was reported to elicit feeding behavior.

Jennings, J.H., Rizzi, G., Stamatakis, A.M., Ung, R.L., and Stuber, G.D. (2013). The inhibitory circuit architecture of the lateral hypothalamus orchestrates feeding. Science *341*, 1517–1521.